2008

The Effect of the Galactic Spheroid on Globular Cluster Evolution

Chigurupati Murali
University of Massachusetts - Amherst

Martin D. Weinberg
University of Massachusetts - Amherst

Recommended Citation
Murali, Chigurupati and Weinberg, Martin D., "The Effect of the Galactic Spheroid on Globular Cluster Evolution" (2008). *Astronomy Department Faculty Publication Series*. 11.
10.1093/mnras/288.3.749

Mon. Not. R. Astron. Soc. **000**, 000–000 (0000) Printed 1 February 2008 (MN LATEX style file v1.3)

The Effect of the Galactic Spheroid on Globular Cluster Evolution

Chigurupati Murali and Martin D. Weinberg⋆
Department of Physics and Astronomy, University of Massachusetts, Amherst, MA 01003-4525, USA

1 February 2008

ABSTRACT

We study the combined effects of relaxation, tidal heating and binary heating on globular cluster evolution, exploring the physical consequences of external effects and examining evolutionary trends in the Milky Way population. Our analysis demonstrates that heating on circular and low-eccentricity orbits can dominate cluster evolution. The results also predict rapid evolution on eccentric orbits either due to strong relaxation caused by the high densities needed for tidal limitation or due to efficient bulge shocking of low density clusters.

The combination of effects leads to strong evolution of the population as a whole. For example, within the solar circle, tidally-limited $10^5 M_\odot$ clusters lose at least 40% of their mass in 10 Gyr. At high eccentricity most of these clusters evaporate completely. Bulge shocking disrupts clusters within 40 kpc which have less than 80% of their mass within their pericentric inner Lagrange point. Our results are consistent with suggestions that the shape of the cluster luminosity function results from evaporation and disruption of low mass clusters; they further predict that the net velocity dispersion of the cluster system in the inner Galaxy has decreased with time. Preliminary constraints on formation models are also discussed. We conclude that the observed cluster system has largely been shaped by dynamical selection.

Key words: globular clusters: general – The Galaxy – galaxies:star clusters – stellar dynamics

1 INTRODUCTION

Many studies of globular cluster evolution have focused on internal mechanisms which drive evolution. This work has produced a clear picture in which initial stellar evolution causes significant mass loss from a nascent cluster (e.g. Chernoff & Weinberg 1990); two-body relaxation leads to mass segregation (e.g. Inagaki & Saslaw 1985) and core collapse in surviving clusters (e.g. Cohn 1980); binary heating halts collapse (e.g. Lee et al. 1991); and the cluster continuously loses mass due to the escape of stars, eventually undergoing complete evaporation (e.g. Lee & Goodman 1995).

It is also recognized that the Galaxy influences cluster evolution. The time-dependent tidal field heats clusters and tidal limitation aids in the removal of escaping stars. Previous investigations have considered disk shocking, bulge shocking and tidal limitation, concluding that each will play a role, particularly in the inner Galaxy (e.g. Spitzer & Chevalier 1973; Chernoff & Shapiro 1987; Aguilar, Hut & Ostriker 1988; Weinberg 1994). In addition, recent observational studies showing correlations of cluster properties with Galactocentric position indicate the measurable influence of the Galaxy (e.g Chernoff & Djorgovski 1989; Djorgovski et al 1993; Djorgovski & Meylan 1994).

The principal tool used in studies of cluster evolution over the last decade-and-a-half has been direct solution of the Fokker-Planck equation (Cohn 1979). However, most of these calculations have excluded external effects. Recently, using time-dependent perturbation theory to investigate disk shocking, Weinberg (1994) demonstrated that resonant forcing can perturb internal stellar trajectories beyond the limit expected from adiabatic invariance. This indicates that the Galaxy plays a greater role in cluster evolution than previously thought and motivates new studies of cluster evolution which combine internal and external effects.

The importance of external heating requires us to reexamine the current picture of internally-driven evolution. In particular, external effects will influence the collapse rates, evaporation times and general physical properties derived in previous calculations. The present work compares this behavior with and without heating over a wide range of

⋆ Alfred P. Sloan Foundation Fellow.

cluster properties to present a revised view. This study also examines the survival and disruption characteristics of clusters on a range of Galactic orbits to shed light on the initial conditions of the cluster system. The results demonstrate that evolution does indeed depend strongly on position and orbit, further implying that observed cluster properties have been largely determined through dynamics.

Our study rests on a linear theory of external heating– based on Weinberg's (1994) treatment of disk shocking– which we include in numerical solutions of the Fokker-Planck equation. Nearly all previous work has emphasized impulsive shock heating due to a single passage through the disk or bulge. The work presented here describes resonant heating due to the time-varying tidal field encountered on periodic orbits of the cluster in the Galaxy- an effect we refer to as *orbit* heating. In this context, shock heating is seen to result from the broad resonances caused by an impulsively applied external force.

Although our treatment of external heating can include the influence of any component of the Galactic potential, here we consider only the spheroid in order to allow precise definition of the physical behavior and preliminary description of the evolutionary trends. The present study includes heating on cluster orbits in the isothermal sphere and is used to study cluster evolution from initial King model states to the point of complete evaporation on a range of orbits in the Galaxy. Our conclusions, therefore, place only lower limits on the overall rate of cluster evolution but are significant nonetheless.

The plan of the paper is as follows. We derive the linear theory of external heating in §2 and discuss its physical interpretation in §3. In §4, the numerical implementation is described. In §5 we present the results of our study of cluster evolution under the combined influence of internal and external effects. Finally, in §6, we discuss the implications of the results for the Milky Way globulars. Readers concerned primarily with the effects of heating and its evolutionary consequences may skip §2 without loss of continuity.

2 DERIVATION OF EXTERNAL HEATING RATE

The physics behind the perturbation theory discussed below can be summarized as follows. Each orbit in the cluster acts like a pendulum with two-degrees of freedom (cf. Binney & Tremaine 1987, Chap. 3). The time-dependent tidal field can drive the pendula at a discrete or continuous spectrum of frequencies depending on whether the perturbation is quasi-periodic or aperiodic, respectively. Because the temporal variation discussed here is caused by the cluster's orbit in the spherical component of the Galaxy, the spectrum is discrete. For disk shocking described by Weinberg (1994), the spectrum is continuous. In both cases, the energy of each orbit changes as it passes through the resonance. The accumulated effect of all possible resonances on all orbits, drives the secular evolution of the equilbrium distribution function (DF). The expressions given below are valid for both periodic and aperiodic cases.

We compute the evolution by expanding the Boltzmann equation to first order and solving for the perturbed distribution function (neglecting self-gravity). The first-order change phase mixes but second order energy input leads to an induced phase space flux which helps drive cluster evolution. N-body comparisons shown in Appendix E indicate that the self-gravity of the tidally-induced wake has negligible effect for cases of interest here.

We use a locally inertial reference frame which is centered on the cluster and has axes fixed in space (see Appendix A for derivation). The unperturbed Hamiltonian is therefore completely separable, implying the existence of action-angle variables. This frame allows the internal dynamics to be defined in accordance with the standard Fokker-Planck technique (e.g. Cohn 1979) which uses an energy-space DF $f(E)$ and depends on the adiabatic invariance of the radial action. Within this framework, we derive a version of the formalism presented by Weinberg (1994) which describes heating of globular clusters on arbitrary orbits in external potentials.

2.1 Perturbed distribution function

The linearized Boltzmann equation is a linear partial differential equation in seven variables. Using action-angle variables, we can separate the equation and employ standard DFs constructed according to Jeans' theorem (Binney & Tremaine 1987). The explicit form of the linearized Boltzmann equation is

$$\frac{\partial f_1}{\partial t} + \frac{\partial f_1}{\partial \mathbf{w}}\frac{\partial H_0}{\partial \mathbf{I}} - \frac{\partial f_0}{\partial \mathbf{I}}\frac{\partial H_1}{\partial \mathbf{w}} = 0, \tag{1}$$

where $\mathbf{w}$ is the vector of angles, and $\mathbf{I}$ are the conjugate actions. The quantities f_0 and H_0 depend on the actions alone. The small variation in Galactic potential over a typical cluster size allows quadratic expansion of the tidal field (see Appendix A for details). We may thus define $H_1 = u(\mathbf{r})g(t)$ and expand in a Fourier series in action-angle variables (e.g. Tremaine & Weinberg 1984). Each term $f_{1\mathrm{l}}$ in the Fourier series is the solution of the following differential equation:

$$\frac{\partial f_{1\mathrm{l}}}{\partial t} + (i\mathbf{l}\cdot\mathbf{\Omega})\mathrm{f}_{1\mathrm{l}} = \mathrm{i}\mathbf{l}\cdot\frac{\partial \mathrm{f}_0}{\partial \mathbf{I}}\mathrm{U}_{\mathrm{l}}(\mathbf{I})\mathrm{g(t)} \equiv \mathrm{i}\mathbf{l}\cdot\frac{\partial \mathrm{f}_0}{\partial \mathbf{I}}\mathrm{H}_{1\mathrm{l}}, \tag{2}$$

where $\mathbf{\Omega} = \partial \mathrm{H}/\partial \mathbf{I}$ and

$$U_{\mathrm{l}}(\mathbf{I}) = \frac{1}{(2\pi)^3}\int_{-\pi}^{\pi} \mathrm{u}(\mathbf{r})\mathrm{e}^{-\mathrm{i}\mathbf{l}\cdot\mathbf{w}}\mathrm{d}^3\mathbf{w}. \tag{3}$$

The inhomogeneous equation may be solved using a Green's function (e.g. Birkhoff & Rota 1962, p.39) to give the time-dependence for each coefficient of the perturbed DF

$$f_{1\mathrm{l}} = i\mathbf{l}\cdot\frac{\partial \mathrm{f}_0}{\partial \mathbf{I}}\mathrm{U}_{\mathrm{l}}(\mathbf{I})\mathrm{e}^{-\mathrm{i}\mathbf{l}\cdot\mathbf{\Omega}\mathrm{t}}\int_{\mathrm{t}_0}^{\mathrm{t}} \mathrm{dt}'\mathrm{e}^{\mathrm{i}\mathbf{l}\cdot\mathbf{\Omega}\mathrm{t}'}\mathrm{g}(\mathrm{t}'), \tag{4}$$

where we have assumed that the perturbation begins at time t_0.

2.2 Heating rate

The rate of change in energy arising from the perturbation follows from Hamilton's equations (Weinberg 1994). The total phase-averaged change in energy can be written as

$$\langle E\rangle = \int_{t_0}^{t} dt \sum_{\mathrm{l}=-\infty}^{\infty} (i\mathbf{l}\cdot\mathbf{\Omega})\mathrm{H}_{1-\mathrm{l}}\mathrm{f}_{1\mathrm{l}}. \tag{5}$$

Substituting for $f_{1\mathrm{l}}$ from equation (4) yields

$$\langle E\rangle = -4\pi^3 \sum_{\mathbf{l}=-\infty}^{\infty} (\mathbf{l}\cdot\mathbf{\Omega})(\mathbf{l}\cdot\frac{\partial \mathrm{f}_0}{\partial \mathbf{I}})|\mathrm{U}_\mathrm{l}|^2 \left| \int_{\mathrm{t}_0}^{\mathrm{t}} \mathrm{dt}' \mathrm{e}^{\mathrm{i}\mathbf{l}\cdot\mathbf{\Omega}\mathrm{t}'} \mathrm{g}(\mathrm{t}') \right|^2, \quad (6)$$

which represents the heat input due to the perturbation during an interval $\Delta t = t - t_0$. This expression is valid for finite-duration, aperiodic perturbations such as disk passage as well as periodic perturbations which arise on regular orbits in the Galaxy. In particular, Weinberg's (1994) results for disk shocking are obtained from equation (6) by substituting the tidal amplitude appropriate to the disk profile for $g(t')$ and integrating over the interval $(-\infty, \infty)$ assuming a linear trajectory.

For periodic perturbations it is more suitable to derive the asymptotic heating rate (e.g. Landau & Lifschitz 1965, p.151). We first expand the tidal amplitude in a Fourier series

$$g(t) = \sum_{n=-\infty}^{\infty} a_n e^{in\omega t}, \quad (7)$$

and substitute into equation (6). Taking the limit $t \to \infty$ and assuming the onset of the perturbation at $t_0 = 0$, we obtain

$$\langle \dot{E}\rangle = -8\pi^4 \sum_{\mathbf{l}=-\infty}^{\infty} (\mathbf{l}\cdot\mathbf{\Omega})(\mathbf{l}\cdot\frac{\partial \mathrm{f}_0}{\partial \mathbf{I}})|\mathrm{U}_\mathrm{l}|^2 \sum_{\mathrm{n}=-\infty}^{\infty} |\mathrm{a}_\mathrm{n}|^2 \delta(\mathrm{n}\omega - \mathbf{l}\cdot\mathbf{\Omega}). \quad (8)$$

Integrating $\langle \dot{E}\rangle$ over inclination and angular momentum, we obtain the change in energy which defines the induced change in the distribution, given by a one-dimensional continuity equation in energy space (appropriate to the 1D Fokker-Planck formulation employed below; see Appendix C for derivation):

$$\frac{\partial f}{\partial t} = \frac{1}{16\pi^2 P(E)} \frac{\partial}{\partial E}\big\{\langle\langle \dot{E}\rangle\rangle\big\}, \quad (9)$$

where $P(E)$ is the phase space volume. This is called the equation of quasilinear diffusion in the plasma literature (e.g. Stix 1992). The term *quasilinear* refers to the proportionality of the heating rate to the squared amplitudes of the linear modes. The linear modes arise from the resonant forcing of stellar orbits by a periodic perturbation. The competition between two-body relaxation and this externally induced phase space flux can strongly influence globular cluster evolution, as we will show below.

2.3 Heating rate in isothermal sphere

Below we will need the heating rate for a cluster orbiting in the isothermal sphere. For most galaxies, the small variation in potential over a typical cluster size allows quadratic expansion of the tidal field. Therefore, the perturbing Hamiltonian is:

$$H_1 = \frac{1}{2}\Omega_0^2(t)\big[-\cos 2\Theta(t)x^2 - 2\sin 2\Theta(t)xy - \cos 2\Theta(t)y^2 + z^2\big], \quad (10)$$

where $\Omega_0(t) = V_0/R(t)$ is the angular rotation speed at the orbital radius at time t and $\Theta(t) = \int_0^t dt'\Omega$ is the instantaneous azimuthal angle of orbit. Using equations (10) and (11) in Weinberg (1994), we can write the perturbation as a series in action-angle variables:

$$H_1 = \frac{1}{2}\Omega_0^2(t) \sum_{\mathbf{l}=-\infty}^{\infty} \big\{ \frac{1}{3}\sqrt{4\pi} V_{000}(\beta)\delta_{l_2 0}\delta_{l_3 0} + \frac{2}{3}\sqrt{\frac{4\pi}{5}} V_{2l_2 0}(\beta)\delta_{l_3 0} - e^{-2i\Theta}\sqrt{\frac{2\pi}{15}} V_{2l_2 2}(\beta)\delta_{l_3 2} - e^{2i\Theta}\sqrt{\frac{2\pi}{15}} V_{2l_2,-2}(\beta)\delta_{l_3,-2}\big\} X_{l_2}^{l_1} e^{i\mathbf{l}\cdot\mathbf{w}}, \quad (11)$$

where

$$X_{l_2}^{l_1} = \frac{1}{2\pi}\int_{-\pi}^{\pi} dw_1 e^{-il_1 w_1} r^2 e^{il_2(\psi - w_2)}, \quad (12)$$

β is the inclination of the orbital plane and $V_{ll_2l_3}(\beta)$ is a rotation matrix (e.g. Tremaine & Weinberg 1984). The angle $\psi - w_2$ is the difference between the mean azimuthal angle w_2 and the azimuthal angle in the orbital plane. We substitute this expansion into equation (8) and average over inclination and angular momentum to derive the heating rate

$$\langle\langle \dot{E}\rangle\rangle = -8\pi^4 \sum_{\mathbf{l}=-\infty}^{\infty} \int d\kappa\kappa J_{max}^2/\Omega_1 (\mathbf{l}\cdot\mathbf{\Omega})(\mathbf{l}\cdot\frac{\partial \mathrm{f}_0}{\partial \mathbf{I}})|\mathrm{X}_{\mathrm{l}_2}^{\mathrm{l}_1}|^2 \left\{ \left[(\frac{1}{18} + \frac{1}{90})\delta_{l_2 0} + \frac{1}{60}\delta_{l_2|2|} \right] \sum_{n=-\infty}^{\infty} |a_n|^2 \delta(\mathbf{l}\cdot\mathbf{\Omega} - \mathrm{n}\omega) + \left[\frac{1}{30}\delta_{l_2 0} + \frac{1}{20}\delta_{l_2|2|} \right] \sum_{n=-\infty}^{\infty} |b_n|^2 \delta(\mathbf{l}\cdot\mathbf{\Omega} - \mathrm{n}\omega) \right\}, \quad (13)$$

where

$$a_n = \frac{1}{P}\int_{-P/2}^{P/2} dt \Omega_0^2(t) e^{-in\omega t}, \quad (14)$$

$$b_n = \frac{1}{P}\int_{-P/2}^{P/2} dt \Omega_0^2(t) e^{-2i\Theta(t) - in\omega t} \quad (15)$$

and P is the period of the cluster orbit.

For an isotropic DF, $\mathbf{l}\cdot\partial \mathrm{f}_0/\partial\mathbf{I} = (\mathbf{l}\cdot\mathbf{\Omega})\mathrm{df}_0/\mathrm{dE}$. We also explore the effect of anisotropy using Merritt-Osipkov models (e.g. Binney & Tremaine 1987). The distribution function takes the form $f_0(\mathbf{I}) = \mathrm{f(Q)}$, where $Q = E \pm J^2/2r_a^2$, $\mathbf{l}\cdot\partial \mathrm{f}_0/\partial\mathbf{I} = df_0/dQ(\mathbf{l}\cdot\mathbf{\Omega} \mp \mathrm{l}_1\Omega_1\mathrm{J}/\Omega_2\mathrm{r}_\mathrm{a}^2 \pm \mathrm{l}_2\mathrm{J}/\mathrm{r}_\mathrm{a}^2)$. The anisotropy increases with decreasing anisotropy radius, r_a.

3 DISCUSSION OF PHYSICAL MECHANISM

A cluster orbiting in the Galaxy feels a time-dependent tidal field. A typical orbit is periodic and introduces a periodic external force on orbits of cluster stars. As described in §2, resonant heating occurs when the periods of stellar orbit and external force coincide, leading to repeated acceleration and increase in the energy of individual orbits. Integrated over many periods, the energy gained by the orbit increases linearly with time (c.f. eq. 8). Energy absorption eventually leads to the evolution of individual orbits. (see Appendix D for discussion and numerical implementation of finite duration resonances). This in turn drives the secular evolution of the cluster potential.

Orbits can either gain or lose energy to the tidal field depending on the particular resonance. For example, in disk galaxies with flat rotation curves it is well-known that the inner Lindblad resonance loses energy to a perturbation while an outer Lindblad resonance gains energy. However, for isotropic distribution functions with $df/dE > 0$, the perturbation always heats the system on average though some localized regions of phase space may lose energy.

Non-resonant interaction has no net effect on an orbit. Successive maxima in the external force tend to accelerate and decelerate the star equally, leading to asymptotic cancellation as long as the initial transients remain linear (i.e. do not alter the intrinsic frequency of the star with an initial jolt). Over short times, non-resonant heating does occur because the time duration is insufficient for complete cancellation to occur.

Non-linear transient or *impulsive* heating leads to rapid change in orbital energies as a rapidly applied force 'kicks' a star regardless of its orbital frequency. However, the standard impulse approximation, when used to describe a periodic perturbation, ignores the long-term decay of transient energy in the linear limit as well as the linear growth in energy at the resonances. For most cases of interest, heating rates are in the linear limit, implying that external influence depends primarily on secular transfer of energy through orbital resonances.

To illustrate the behavior of transients and transient decay, Figure 1 compares the exact time-dependent energy input given by equation (6) with the energy input defined by the asymptotic heating rate equation (8). Transients decay rapidly at low energy and more slowly at high energy. Empirically, we find that two to three Galactic orbital periods are required before the asymptotic limit is effectively reached. This treatment therefore adequately describes all but the outermost halo clusters for which initial transients may still be important. The comparisons of perturbation theory with N-body simulation shown in Appendix E demonstrate the validity of the approach.

The magnitude of the heating rate is determined by the cluster profile, density and orbit. The profile and density define the distribution of internal orbital frequencies and the cluster orbit defines the external forcing frequencies and amplitude. For a cluster of fixed profile and mass, the density is determined by the tidal radius. Individual clusters may not be tidally limited due to initial conditions or heating-driven expansion. Therefore we use the function $M(x_p)$ to parameterize the fraction of the total cluster mass enclosed within the instantaneous pericentric inner Lagrange point, x_p. This function depends on the profile and the ratio of cluster mean density to the mean density required by tidal limitation. A tidally-limited cluster has limiting radius, $R_c = x_p$, and therefore $M(x_p) = 1$, while a tidally-unlimited has $R_c > x_p$ and therefore $M(x_p) < 1$. Heating rates for a given orbit increase as $M(x_p)$ decreases.

The perturbing potential in the logarithmic sphere, equation (10), heats clusters on orbits of any eccentricity. The tide transfers energy and angular momentum to the cluster through the resonances, which unbinds stars. On circular orbits, the tidal field creates a triaxial perturbation of constant amplitude proportional to Ω_0^2 rotating with fixed pattern speed Ω_0. On eccentric orbits, conservation of center-of-mass angular momentum introduces time-dependent amplitude and rotation rate. This produces more resonances. Tidal torquing can also induce a net spin.

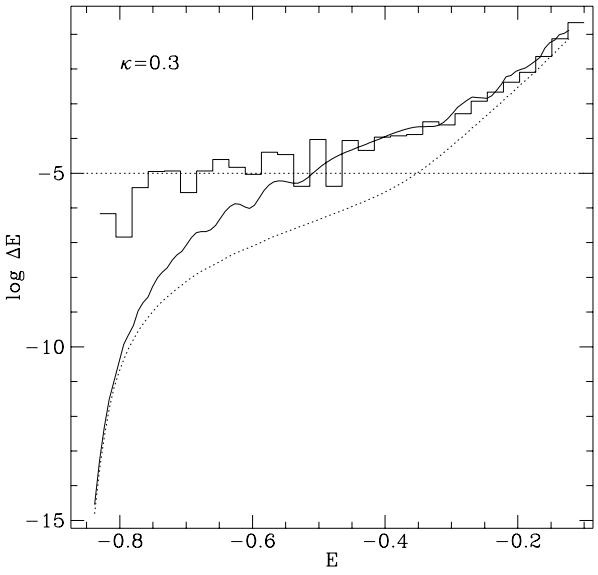

Figure 1. The mean change in energy as a function of internal orbital energy in a $W_0 = 5$ King model due to heating on an eccentric $\kappa = 0.3$ ($e \approx 0.7$) orbit after one orbital period. Comparison of simulation (histogram), exact time-dependent perturbation theory (equation 6, solid) and heat input calculated from asymptotic heating rate (equation 8, dotted) shows that initial transients decay strongly at low energy while impulsive energy change persists at high energy. Horizontal dotted line indicates the level of accuracy in the simulation.

The rate of external heating is also influenced by our choice of equilibrium phase space distributions. For example, according to Jeans' theorem, one can define equilibria in the rotating frame of a circular cluster orbit using the Jacobi constant, E_J (e.g. Heggie & Ramamani 1994). By transforming to the frame in which the perturbation is time-independent, we remove the resonances from the problem. We can therefore choose a bound distribution of orbits in E_J using the limiting zero-velocity surface, so no stars are lost and the cluster experiences no net tidal heating, although inertial energies and angular momenta are not conserved. Using $f(E)$ instead of $f(E_J)$ leads to heating in the analogous case because we cannot choose orbits which are strictly bound. In any case, a real cluster cannot reach true equilibrium because it is bound and therefore undergoes relaxation. In fact, as is shown below, it is typically a competition between external heating and relaxation due to strong resonances with diffused core stars that strongly influences cluster evolution.

4 FOKKER-PLANCK CALCULATIONS

To determine the influence of external heating on cluster evolution, we conduct a series of Fokker-Planck calculations which begin with King model initial conditions and run through core collapse to complete evaporation. Relaxation is computed using the multi-mass code of Chernoff &

Weinberg (1990) which solves Henon's (1961) orbit-averaged Fokker-Planck equation. Core heating is included in the form described by Lee et al (1991) with a time step that supresses stochastic core osillations. Implementation of external heating is detailed in Appendix D. The comparisons shown in Appendix E are used to test the implementation.

Each physical process depends on the input model parameters listed in Table 1. The total mass is denoted by M_c and the concentration by W_0. Orbits in the isothermal sphere are defined by their energy E and angular momentum J. In place of absolute angular momentum J, we use the relative angular momentum $\kappa = J/J_{max}(E)$, where $J_{max}(E)$ is the angular momentum of a circular orbit with energy E. The value $\kappa = 0$ denotes a radial orbit and the value $\kappa = 1$ denotes a circular orbit. The apocentric, pericentric and mean orbital radii are denoted R_a, R_p, R_{av}, respectively. We represent the Galactic potential as a singular isothermal sphere with rotation velocity $v_0 = 220$ km/s.

We consider a range of initial values for $M(x_p)$. If the young, rich LMC clusters are representative of young globular clusters, $M(x_p)$ may be significantly smaller than unity initially (Elson, Fall & Freeman 1987). Furthermore, as discussed in §5.4.2, formation scenarios can imply varying degrees of tidal truncation for an individual cluster depending on the local conditions under which it forms and the orbit on which it travels.

The distribution of stellar masses in the cluster is given by a power-law mass spectrum, $dN/dM \propto m^{-\alpha}$, with upper and lower mass limits m_l and m_u, respectively. Fiducial values $\alpha = 2.35$, $m_l = 0.1$ and $m_u = 2.0$ are adopted in §5.1 to represent the cluster mass spectrum following the period of strong stellar evolution when relaxation, tidal heating and binary heating dominate cluster evolution. The importance of stellar evolution diminishes after ~ 1 Gyr for $\alpha = 2.35$ and $m_l = 0.1$ which corresponds to the main sequence lifetime for a $2M_\odot$ A-star. The effect of changing the mass spectrum is explored in §5.2.

5 RESULTS

5.1 Orbital heating and bulge shocking

Because heating rates depend on cluster profile, tidal truncation and orbit, comparisons in different physical regimes are needed to demonstrate the primary influences of heating on cluster evolution. We choose four specific examples listed in Table 2.

Example 1 compares the relative strengths of heating rates on different orbits using physically identical clusters, each of which is tidally-limited at its orbital pericenter. In this case, because the average tidal strength is largest on circular orbits, heating is also strongest on circular orbits and decreases with eccentricity (Figure 2).

To investigate the effect of heating on long-term evolution, we compare evaporation times, t_{ev}, for tidally limited clusters of different mass, concentration and κ. Table 3 shows t_{ev} normalized by the circular, $10^5 M_\odot$ $W_0 = 5$ case (arbitrary scaling to physical units is provided in §5.4.1). In these comparisons, clusters of a particular mass and concentration are identical and clusters of differing mass and concentration possess the mean density required for tidal limitation.

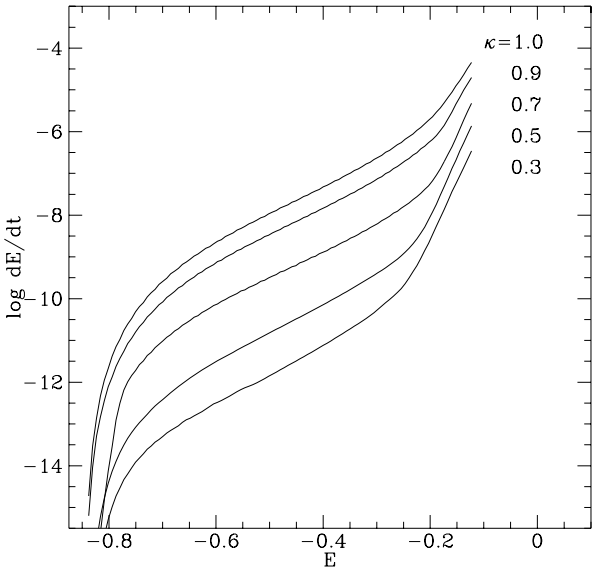

Figure 2. Example 1: comparison of heating rates in identical tidally-limited $W_0 = 5$ clusters on different orbits. Values of κ are indicated to the right of each curve. Heating on circular orbits dominates because the average tidal strength is highest, decreasing with eccentricity because average tidal amplitude drops monotonically. Heating rates in circular and $\kappa = 0.3$ case differ by about 2 orders of magnitude. In the circular case, orbits near the tidal boundary gain $\sim 10\%$ in energy in an orbital time.

For identical clusters, t_{ev} decreases monotonically with κ, reaching a minimum for circular orbits. Evaporation times can decrease by a factor of two in circular cases when tidal heating is included. The relative evaporation times reflect the relative strength of heating rates shown in Figure 2. Heating accelerates evolution because external forcing efficiently torques and expels high-energy core stars on radial orbits, as noted by Oh & Lin (1992) in N-body calculations. This reduces the local relaxation time in the core, enhances relaxation rates and causes rapid evaporation. Spitzer & Chevalier (1973) noted this effect in certain regimes of disk shocking, interpreting it as an increase in the core-halo temperature gradient (see also Chernoff & Shapiro 1987, Weinberg 1994). For the highest eccentricities, t_{ev} is only slightly shorter than with no heating, demonstrating the insignificance of high-eccentricity heating in tidally-limited clusters.

In many cases, evaporation time does not vary strongly with concentration for the same orbit and mass, indicating that overall mass loss rates are insensitive to initial concentration. In the exceptional $\kappa = 0.9$ and 1.0, $W_0 = 3$, $10^6 M_\odot$ cases, heating causes rapid disruption because these clusters have low binding energy and long relaxation times and are easily torn apart by the tide.

While Example 1 compares heating rates as a function of eccentricity in identical clusters, the orbits occupy different regions of the Galaxy (c.f. Table 2). In Example 2, we consider clusters in similar regions by comparing tidally-limited clusters on orbits of equal mean radius. Because they are tidally truncated, these clusters still undergo the same rate of heating relative to internal energies shown in Figure

Table 1. Processes and parameter dependences

	Parameters							
Process	α	m_l	m_u	W_0	$M(x_p)$	M_c	E	κ
Relaxation	√	√	√	√	√	√		
External Heating				√	√	√	√	√
Core Heating	√	√	√	√	√	√		

Table 2. Example scenarios for a $10^5 M_\odot$ cluster

Example	κ	R_a (kpc)	R_p (kpc)	P (100Myr)	r_t (pc)	x_p (pc)	$M(x_p)$	$t_{dyn}(10^6 yr)$
1	1.0	8.5	8.5	2.5	70	70	1.0	5.0
	0.9	11.2	9.2	2.1	70	70	1.0	5.0
	0.7	19.6	10.3	3.1	70	70	1.0	5.0
	0.5	37.8	11.8	5.3	70	70	1.0	5.0
	0.3	89.4	13.7	11.3	70	70	1.0	5.0
2	1.0	8.5	8.5	2.5	70	70	1.0	5.0
	0.9	9.4	7.6	1.8	63.5	63.5	1.0	4.3
	0.7	10.9	5.7	1.7	48.5	48.5	1.0	2.9
	0.5	11.9	3.7	1.7	33.2	33.2	1.0	1.6
	0.3	12.4	1.9	1.6	19.3	19.3	1.0	0.7
3	1.0	8.5	8.5	2.5	70	70	1.0	5.0
	0.9	9.4	7.6	1.8	70	61.4	1.0	5.0
	0.7	10.9	5.7	1.7	70	47.6	0.99	5.0
	0.5	11.9	3.7	1.7	70	31.5	0.92	5.0
	0.3	12.4	1.9	1.6	70	16.4	0.63	5.0
4	0.3	15.0	2.3	1.9	22.9	22.9	1.0	0.9
	0.3	15.0	2.3	1.9	41.3	23.5	0.95	2.3
	0.3	15.0	2.3	1.9	48.8	21.1	0.9	2.9
	0.3	15.0	2.3	1.9	61.1	20.3	0.8	4.1
	0.3	15.0	2.3	1.9	73.2	19.4	0.7	5.4

2. However, cluster densities vary due to differences in orbital angular frequencies. For fixed cluster mass, this implies that tidal radii will vary.

The tidal radius r_t decreases with the increased perigalactic angular frequency at higher eccentricity. This increases the mean density and decreases the dynamical time t_{dyn}, producing shorter relaxation times, larger evaporation rates and, as a result, shorter lifetimes as compared to Example 1. A cluster with $\kappa = 0.3$ in Example 2 will evaporate in 1/7 the time of a cluster with $\kappa = 0.3$ in Example 1 and 1/5 the time of a cluster with $\kappa = 1.0$ (the circular case).

Since cluster orbits are generally unknown, the degree of tidal truncation at pericenter cannot be directly inferred. So, in Example 3, we assume that an observed cluster lies at its average orbital radius for a range of eccentricity and is tidally limited for zero eccentricity. The mass within the pericentric inner Lagrange point $M(x_p)$ can be substantially less than unity on eccentric orbits (Table 2). This leads to stronger heating than found on the same orbits in Example 1 (see Figure 3). For $\kappa = 0.7$ the heating rate is much larger than in Example 1 even though only small amounts of mass overlie x_p. For $\kappa = 0.3$ strong impulsive heating or bulge shocking (e.g. Aguilar et al 1988) occurs due to the increase in tidal amplitude.

Example 4 shows the dependence of heating rates on degree of tidal truncation for a fixed $\kappa = 0.3$ orbit. Figure 4 illustrates the dependence of heating on both κ and $M(x_p)$: significant heating will occur on orbital timescales for $\kappa = 0.3$ and $M(x_p) < 0.9$. Strong heating for $\kappa > 0.3$ will also occur because these orbits have larger heating rates for the same value of $M(x_p)$. Table 2 shows the variation in cluster size and dynamical time with tidal truncation, indicating the corresponding variation in mean density.

The evolutionary consequences of the heating rates in Example 4 are shown in Table 4. Clusters of different mass and concentration have equal $M(x_p)$ on the same orbit. Weakly bound clusters disrupt more easily because the resonances occur more deeply within the system. Survival of $W_0 = 3$ clusters decreases strongly with $M(x_p)$. Conversely, for small reduction in $M(x_p)$, survival of $W_0 = 5$ and $W_0 = 7$ clusters is enhanced as increased heating is offset by diminished relaxation. For $W_0 = 5$, maximum enhancement occurs at $M(x_p) \sim 0.95$. For $W_0 = 7$, higher binding energies lead to even longer lifetimes for more severe truncations. Further reductions in $M(x_p)$ eventually lead to rapid disruption due to strong tidal shocking.

These results define a rough criterion for bulge shocking: for $W_0 \leq 5$ and $\kappa > 0.3$, bulge shocking will occur for

Table 3. Evaporation times t_{ev}

$W_0 = 3$	κ				
M_c ($M_\odot$)	1.0	0.9	0.6	0.3	nh[a]
1.0×10^5	0.65	0.95	1.27	1.29	1.30
1.0×10^6	0.94	3.69	9.61	10.9	11.2
$W_0 = 5$	κ				
M_c ($M_\odot$)	1.0	0.9	0.6	0.3	nh
1.0×10^5	1.00	1.15	1.34	1.37	1.38
5.0×10^5	3.20	4.25	5.64	6.10	6.20
1.0×10^6	5.20	7.01	10.31	11.43	11.82
$W_0 = 7$	κ				
M_c ($M_\odot$)	1.0	0.9	0.6	0.3	nh
1.0×10^5	1.12	1.27	1.40	1.41	1.42
5.0×10^5	3.97	4.70	5.95	6.25	6.37
1.0×10^6	6.35	8.29	11.06	11.96	12.13

[a] nh denotes no heating

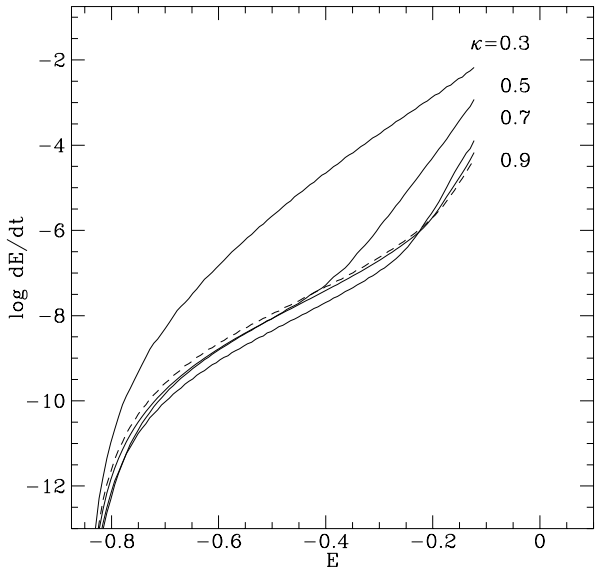

Figure 3. Heating rates for Example 3. Tidally-limited circular case (dashed line) is plotted for reference. For $\kappa = 0.7$, heating increases strongly in mildly tidally-unlimited cluster compared to Example 1. For $\kappa = 0.3$, distribution with $E > -0.3$ undergoes strong shocking on orbital time scale.

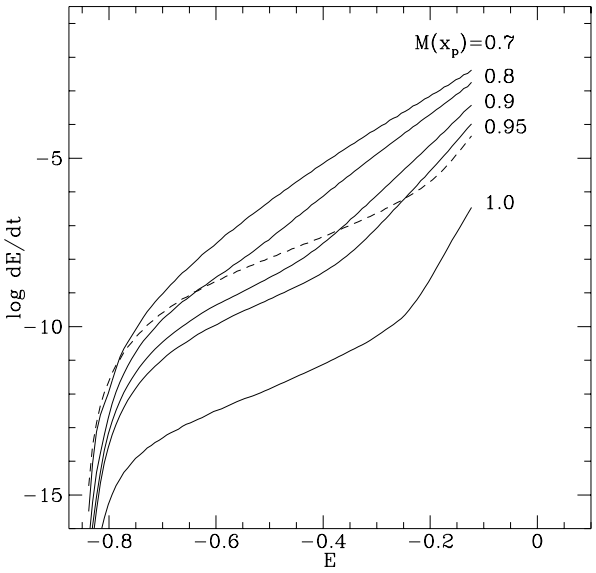

Figure 4. Heating rates for Example 4. Shocking develops slowly as $M(x_p)$ decreases. For $M(x_p) \sim 0.95$ heating of the tail is slightly stronger than in the tidally-limited circular case (dashed line). Heating at low energies is substantially less. Strong impulsive heating or bulge shocking of the tail of the distribution will occur for $M(x_p) < 0.9$.

$M(x_p) < 0.9$. Disruption for fixed $M(x_p)$ and κ also implies disruption for larger κ because heating rates increase with κ. For $\kappa < 0.3$, bulge shocking requires even smaller $M(x_p)$ to cause disruption.

This series of comparisons establishes three important aspects of tidal effects on different orbits in a spherical potential: 1) low-eccentricity and circular orbit heating for tidally-limited clusters strongly accelerate evolution; 2) high-eccentricity heating has little effect in tidally-limited cases but the high mean density found for typical orbital radii in the Galaxy leads to short relaxation and evaporation times; 3) high-eccentricity heating, or bulge shocking, becomes important when clusters are tidally-unlimited, although the exact effect depends on $M(x_p)$, κ, W_0 and M_c.

Finally, an important consequence of strong tidal heat-

Table 4. Bulge shocking evaporation times (Example 4)

$W_0 = 3$			$M(x_p)$		
M_c ($M_\odot$)	1.0	0.95	0.9	0.8	0.7
1.0×10^5	1.3	1.3	1.1	0.4	0.2
1.0×10^6	10.9	2.4	0.8	0.4	0.4
$W_0 = 5$			$M(x_p)$		
M_c ($M_\odot$)	1.0	0.95	0.9	0.8	0.7
1.0×10^5	1.4	2.4	2.1	1.0	0.5
1.0×10^6	11.4	12.1	5.2	1.5	0.5
$W_0 = 7$			$M(x_p)$		
M_c ($M_\odot$)	1.0	0.95	0.9	0.8	0.7
1.0×10^5	1.4	2.7	2.4	2.3	2.0
1.0×10^6	12.0	16.0	23.4	13.8	7.5

ing is suppression of the gravothermal instability. Although this may cause expansion and disruption, relaxation slows the expansion and can still produce mass segregation (Figure 5). Therefore, *mass segregation does not necessarily imply core collapse*, a possibility that does not arise when neglecting external heating (e.g. Chernoff & Weinberg 1990; Drukier, Richer & Fahlman 1992). Observed clusters with King profiles and strong mass segregation (such as M71) may reflect the influence of strong tidal effects.

5.2 Influence of Mass Spectrum

The mass spectrum controls the rate of relaxation and interplay with external heating. Clusters with steep mass spectra or a narrow range of low mass stars have lower relaxation rates than do clusters with shallow mass spectra or a wide range in stellar mass (e.g. Chernoff & Weinberg 1990). Here we examine the competition between external heating and relaxation over a range in α and m_u in unheated and circularly heated tidally-limited clusters.

Circular heating reduces evaporation times over a range in α (Table 5). Roughly a factor of three reduction can occur for $\alpha = 3.35$. Differences between heated and unheated clusters increase with α because the slower relaxation rates at high α are more readily enhanced. In addition, for fixed mass and concentration, heating reduces differences in evaporation time which depend on α.

Heating also reduces core collapse times t_{cc} up to 33% (Table 5) and masses remaining at core collapse up to a factor of two (Table 6). High concentration clusters maintain the same core collapse times in all cases but show decreased mass at core collapse.

The non-monotonic behavior of core collapse time with spectral index was also found by Inagaki (1985 Table II) in Plummer law initial profile and Chernoff & Weinberg (1990 Table 4) in King models. This indicates a complex relation between concentration, mass segregation and core collapse. Heating supresses this behavior for $W_0 = 5$.

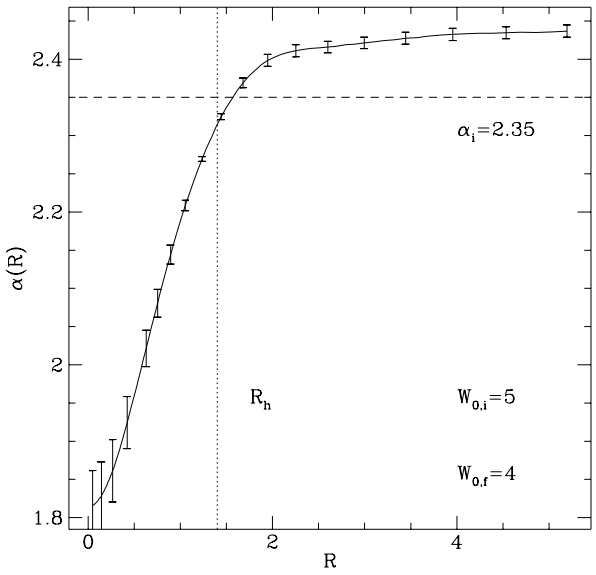

Figure 5. The radial dependence of the mass spectral index for a cluster dominated by bulge shocking: $W_0 = 5$, $M_c = 10^6 M_\odot$, $M(x_p) = 0.8$. α_i is the initial spectral index. R_h is the half-mass radius. Tidally disrupting clusters may show evidence of mass segregation. In this case bulge shocking suppresses core contraction, leading to expansion and disruption. The profile is approximately $W_0 = 4$ and the remaining mass is $M_c = 2.3 \times 10^5 M_\odot$.

Evaporation times decrease with increasing m_u (Figure 6). The decrease in t_{ev} with increasing mass range results from enhanced relaxation caused by a more extreme mass segregation instability. A 25% range in the duration of strong stellar evolution for $\alpha = 2.35$ gives a range in mass limits of $1.9 \leq m_u \leq 2.2$ and results in very small differences in evaporation time.

Table 5. Times of core collapse and evaporation

$W_0 = 5$		α		
M_c ($M_\odot$)	1.35	2.35	3.35	
		t_{ev}		
5.0×10^5	2.7	3.2	5.3	heated
	4.4	6.3	14.1	unheated
1.0×10^6	4.3	5.2	8.2	heated
	8.6	12.3	25.9	unheated
		t_{cc}		
5.0×10^5	1.6	1.6	2.1	heated
	2.2	1.9	2.3	unheated
1.0×10^6	2.7	2.7	3.6	heated
	4.0	3.1	4.4	unheated
$W_0 = 7$		α		
M_c ($M_\odot$)	1.35	2.35	3.35	
		t_{ev}		
5.0×10^5	2.8	4.0	7.4	heated
	4.3	6.1	14.0	unheated
1.0×10^6	4.9	6.4	11.8	heated
	8.1	12.1	26.8	unheated
		t_{cc}		
5.0×10^5	0.56	0.37	0.41	heated
	0.59	0.37	0.38	unheated
1.0×10^6	1.06	0.71	0.76	heated
	1.06	0.71	0.76	unheated

$m_l = 0.1 M_\odot$, $m_u = 2.0 M_\odot$

Table 6. Mass at core collapse

$W_0 = 5$		α		
M_c ($M_\odot$)	1.35	2.35	3.35	
5.0×10^5	0.39	0.54	0.59	heated
	0.65	0.88	0.93	unheated
1.0×10^6	0.30	0.43	0.50	heated
	0.65	0.88	0.93	unheated
$W_0 = 7$		α		
M_c ($M_\odot$)	1.35	2.35	3.35	
5.0×10^5	0.82	0.90	0.92	heated
	0.93	0.98	0.99	unheated
1.0×10^6	0.78	0.87	0.90	heated
	0.93	0.98	0.99	unheated

$m_l = 0.1 M_\odot$, $m_u = 2.0 M_\odot$

5.3 Influence of Anisotropy

Another internal property that determines the influence of external heating is the anisotropy of the stellar orbit distribution. Figure 7 shows the variation of heating rate with anisotropy radius within a cluster. Heating increases with anisotropy due to efficient impulsive heating of radial orbits at apocenter. However, heating rates for $r_a = 2.5$ unbind orbits with $E > -0.25$ in one orbital period t_{cr} and quickly alter the DF. The relaxation time is roughly 100 crossing times, so diffusion cannot maintain the assumed level of radial anisotropy in the cluster halo. We estimate that anisotropy radii of $r_a \geq 5.0$ are sustainable through relaxation. The interplay between heating and anisotropy seen here provides strong incentive to study the evolution of fully anisotropic DFs.

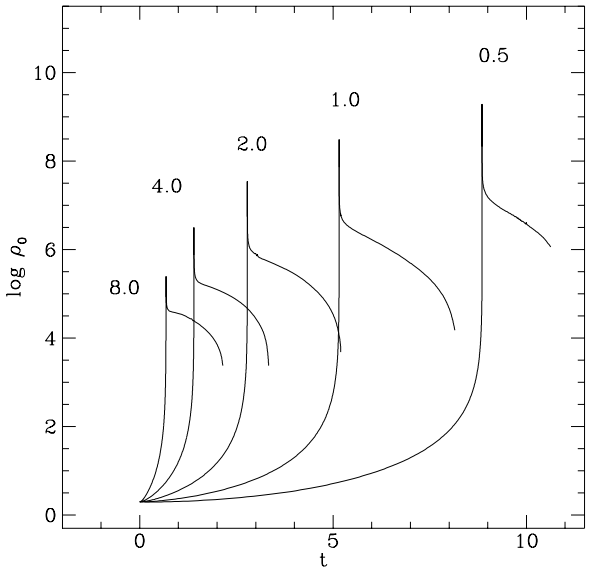

Figure 6. Central density evolution for $W_0 = 5$, $10^6 M_\odot$ clusters on circular orbits with $\alpha = 2.35$, $m_l = 0.1$ and m_u as indicated. Evaporation occurs at the termination of each central density curve. Evaporation times vary by no more than 10% for the expected range $1.9 \leq m_u \leq 2.2$ in initial upper mass limit for $\alpha = 2.35$. Evaporation times decrease with increases mass m_u due to the enhanced mass segregation instability.

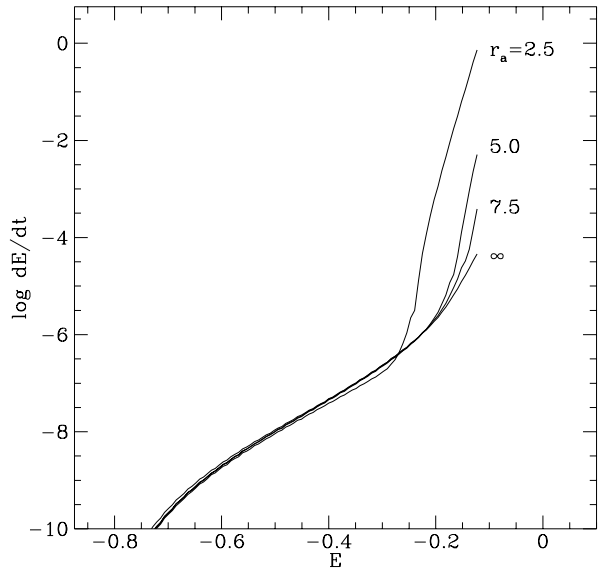

Figure 7. Heating rates are shown for clusters on circular orbits with indicated anisotropy radius. For $r_a = 2.5$, the anisotropy parameter $\beta = 1 - \bar{v}_\theta^2/\bar{v}_r^2 = 0.17$ at the half-mass radius. Energy input increases due to efficient impulsive heating of radial stellar orbits at apocluster.

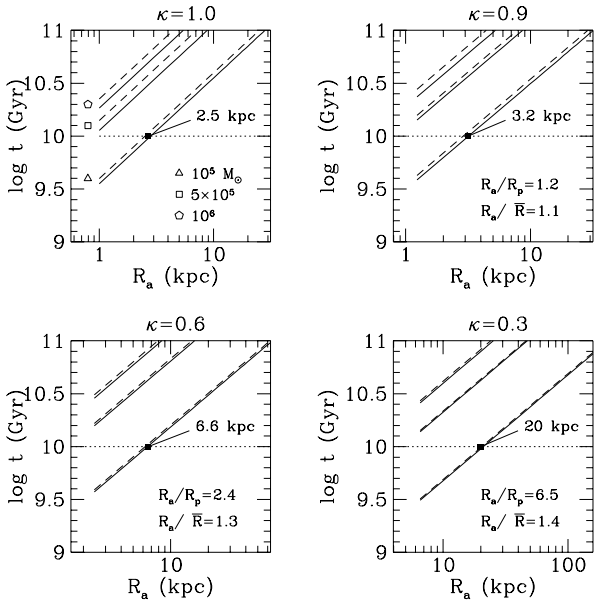

Figure 8. Evaporation times vs. apogalacticon for $W_0 = 5$ (solid) and $W_0 = 7$ (dashed). Low mass clusters evaporate within 10 Gyr in inner Galaxy to apogalactic radii as shown. Strong heating drives low eccentricity clusters to evaporation while high densities of tidal limitation drive high eccentricity clusters to evaporation. Evaporation of $\kappa = 0.3$, $10^5 M_\odot$ occurs out to average radii of 15 kpc.

5.4 Evolution in the Milky Way

5.4.1 Scaled evaporation times

The dimensionless evaporation times for tidally-limited clusters discussed in §5.1 may be scaled to physical units using the following relation

$$t_{phys} = 1.1 \times 10^3 \bar{t} \times t_{ev}, \tag{16}$$

where $\bar{t}$ is the orbital period at the tidal radius

$$\bar{t} = \left(\frac{GM_c}{r_t^3} \right)^{-1/2} \tag{17}$$

and

$$r_t = \left(\frac{GM_c}{2\Omega_p'^2} \right)^{1/3}. \tag{18}$$

The quantity $\Omega_p'(\kappa, R_a)$ is the effective perigalactic angular frequency of an orbit of given κ and apocentric radius R_a due to tidal strain and centrifugal force (defined in Appendix B).

As an example, the dimensionless evaporation times given in Table 3 are scaled to a range of apogalactica in Figure 8. Clusters evaporate over a wide range of Galactocentric radii depending on κ. In 10 Gyr, clusters on circular orbits evaporate within 3 kpc, while those on $\kappa = 0.3$ orbits evaporate out to average radii of 15 kpc.

5.4.2 Survival and disruption

Here we present a simple evolutionary scenario in which clusters form at apocenter with a range of mean density param-

eterized by $\rho_{crit,FR}(R)$, the Fall-Rees (1985) critical cloud density at Galactocentric radius R. This parameterization is chosen to allow normalization with respect to a particular model. Other models (e.g. Harris & Pudritz 1994; Murray & Lin 1992) can be similarly evaluated given expressions for initial protocloud densities as a function of Galactocentic radius. A range of density is used to define a range of $M(x_p)$ for clusters at each radius, thereby illustrating characteristics which are independent of any particular model. We only consider relaxation, external heating and binary heating although gas removal and stellar evolution will play an important role following formation. These effects should weaken the potential and increase disruptive tendencies described here.

In the first case, clusters form on eccentric $\kappa = 0.3$ orbits (e.g. Eggen, Lynden-Bell and Sandage 1962). Figure 9 shows the resulting pattern of survival, disruption and evaporation for 10^5 and $10^6 M_\odot$ clusters after 10 Gyr. Clusters initially with $10^5 M_\odot$ do not surive within $R_{av} = 15$, reflecting the evaporation times shown above. Lower density clusters suffer disruption to even larger distances. High mass clusters with $M(x_p) \lesssim 0.8$ can suffer disruption but none can evaporate.

Cluster formation on less eccentric $\kappa = 0.7$ orbits shows the same qualitative pattern of survival, evaporation and disruption as above (Figure 10). The consequences are less severe because the density contrast between formation at apocenter and tidal limitation at pericenter is not as great. In this case, low mass cluster survival is limited to regions beyond 5 kpc for clusters which are nearly tidally-limited.

6 IMPLICATIONS FOR MILKY WAY CLUSTERS

The calculations presented above bear on our understanding of the observed mass and space distributions of Galactic globular clusters. We summarize some relevant properties for reference. In the Djorgovski (1993) compilation, 65% of 130 clusters with distance estimates lie within the solar circle. The overall peak of the luminosity function of Galactic globulars is $M_v = -7.36$ (Harris 1991) corresponding to a mass of $1.5 \times 10^5 M_\odot$ (where $M/L_v = 2$). The luminosity function varies little in this inner region.

Our results imply that the observed characteristics of this inner population have evolved with time. Because $10^5 M_\odot$ clusters evaporate or lose large amounts of mass in a Hubble time in the inner Galaxy, clusters at the peak of the luminosity function have evolved from higher mass. For example, at 6 kpc clusters on circular orbits with $M_v = -7.36$ will evolve to $M_v = -6.8$ in 10 gyr, losing roughly 40% of their initial mass. Inside the solar circle, clusters near the present peak had at least 30% more mass, depending on the orbit.

Many clusters will also have vanished. We predict that evaporation and disruption of $10^5 M_\odot$ clusters occur within 3 kpc for $\kappa = 1.0$ and within apocentric radii $R_a = 20$ kpc for $\kappa = 0.3$. For intermediate κ, the destruction region is bracketed by these limiting cases. These results buttress arguments based on two-body relaxation times that the shape of the luminosity function stems from evaporation and disruption of a larger initial population of low mass clusters (e.g. Larson 1996, Okazaki & Tosa 1995).

The dependence of survival on orbit implies that the kinematic distribution of clusters has evolved as well. Clusters on high eccentricity orbits in the inner Galaxy are least likely to survive due to both evaporation and bulge shocking. This suggests a decrease in the net velocity dispersion for the rotating system of metal-rich and inner halo metal-poor clusters (Zinn 1993). This tendency may also partially account for observed differences between the kinematics of halo field stars and metal-poor globular clusters (e.g. Aguilar et al. 1988).

Finally, survival also depends strongly on initial cluster densities. Destruction is more pronounced for clusters with low initial density and low initial concentration due to bulge shocking. Bulge shocking can disrupt massive $10^6 M_\odot$ clusters on eccentric orbits out to 40 kpc provided $M(x_p) \lesssim 0.8$. However, a proper assessment of the initial distribution of cluster densities requires cosmogonical considerations.

We conclude that the segment of the cluster population which is native to the Milky Way or which was accreted at an early time represents a dynamically selected sample, with current masses, orbits and densities all favored for survival over a Hubble time of evolution. Tidal interaction with the Galactic disk will amplify these effects. Details will be described in a subsequent paper.

7 SUMMARY

The key conclusions are as follows:

(i) Time-dependent heating on low-eccentricity orbits accelerates evolution and sharply reduces evaporation times.

(ii) Tidally limited clusters on high-eccentricity orbits have high internal density, leading to short evaporation times even though heating rates are negligible.

(iii) Bulge shocking on high-eccentricity orbits can rapidly disrupt clusters over a wide range in mass and apogalactic radius when their densities are roughly a factor of 10 below the mean density required for tidal limitation.

(iv) Evaporation and disruption have shaped the mass, orbit and density distribution of clusters. In particular, clusters at the peak of the luminosity function had at least $\sim 30\%$ more mass depending on orbit. Evaporation on high-eccentricity orbits has decreased the velocity dispersion in the cluster kinematic distribution.

Secondary results are as follows:

(i) Evaporation times do not strongly depend on concentration in most cases. However, heating can lead to rapid disruption in massive clusters with low concentration because of the low binding energy and long relaxation time.

(ii) Clusters disrupting due to heating may still show signs of mass segregation due to continued relaxation.

(iii) Heating accelerates evolution over a range of mass spectral index and reduces the dependence of evaporation time on different initial mass spectra.

(iv) The development of anisotropy through relaxation in the core will increase evolutionary rates found in the isotropic distributions investigated here.

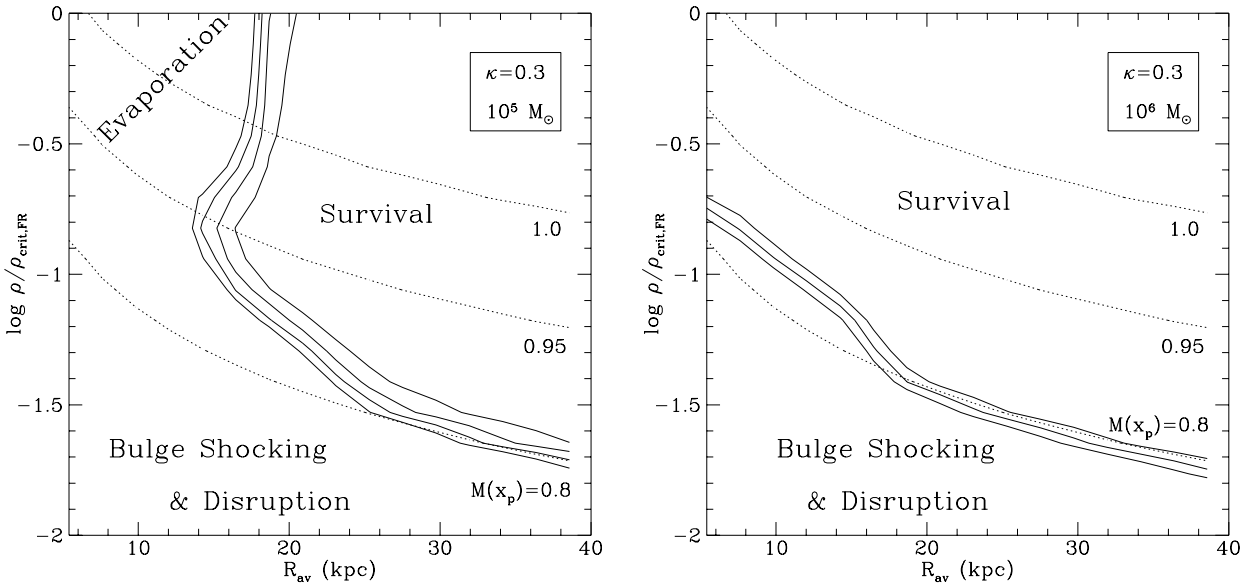

Figure 9. Contours of log mass (solid) show survival and disruption of proto-clusters with an initial $W_0 = 5$ profile after 10 Gyr due to tidal effects on$\kappa = 0.3$ orbits. Contours are in the range $3.75 \leq \log M \leq 4.5$. R_{av} indicates average orbital radius and $\rho_{crit,FR}$ is the Fall-Rees (1985) critical cloud density at radius R. Dotted contours show lines of equal $M(x_p)$. Left: $10^5 M_\odot$ clusters with $\rho \approx \rho_{crit,FR}(R)$ evaporate due to high initial densities, lower density clusters disrupt from bulge shocking and clusters with $M(x_p) \sim 0.95$ survive longest due to balance between heating and relaxation. Right: a density of $0.1\rho_{crit,FR}$ leads to bulge shocking and disruption in $10^6 M_\odot$ out to $R_{av} \sim 10kpc$.

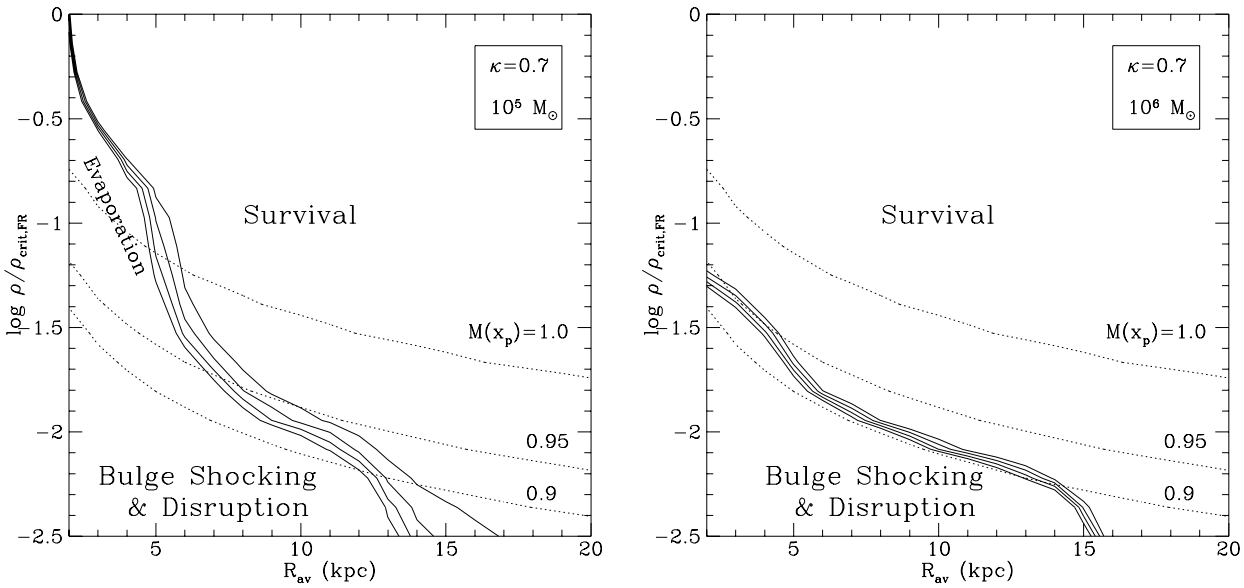

Figure 10. As in Fig. 8 but on $\kappa = 0.7$ orbits. Left: high density $10^5 M_\odot$ clusters evaporate, low density clusters disrupt due to extreme tidal heating and clusters survive at larger radii. The convergence of contours into the upper left corner is a numerical artifact caused by mean densities beyond the range of our calculations. However, these clusters also evaporate because of the high densities. Right: low density clusters disrupt at densities roughly 30% of the mean density for tidal limitation out to 15 kpc due to strong tidal heating

ACKNOWLEDGEMENTS

This work was supported in part by NASA award NAGW-2224.

REFERENCES

Aguilar, L., Hut, P. & Ostriker, J. P. 1988, ApJ, 335, 720
Binney, J. J. & Tremaine, S. D. 1987, Galactic Dynamics, (Princeton: Princeton U. Press)
Bracewell, R. N. 1986, The Fourier Transform and its Applications, (New York: McGraw Hill)
Chandrasekhar, S. 1942, Principles of Stellar Dynamics, (Chicago: Univ. Chicago Press)
Chernoff, D. F. & Djorgovski, S. G. 1989, ApJ, 339, 904
Chernoff, D. F., Kochanek, C. S. & Shapiro, S. L. 1986, ApJ, 309, 183
Chernoff, D. F. & Shapiro, S. L. 1987, ApJ, 322, 113
Chernoff, D. F. & Weinberg, M. D. 1990, ApJ, 351, 121
Cohn, H. N. 1979, ApJ, 234, 1036
Cohn, H. N. 1980, ApJ, 242, 765
Cohn, H. N. 1985, in Dynamics of Star Clusters, eds. Goodman, J., and Hut, P., (Boston: D. Reidel Publishing)
Djorgovski, S., Piotto, G. & Capaciolli, M. 1993, AJ, 105, 2148
Djorgovski, S., & Meylan, G. 1994, AJ, 108, 1292
Drukier, G. A., Fahlman, G.G. & Richer, H. B. 1992, ApJ, 386, 106
Eggen, O. J., Lynden-Bell, D. & Sandage, A. 1962, ApJ, 136, 748
Elson, R. A. W., Fall, S. M. & Freeman, K. C. 1987, ApJ, 323, 54
Elson, R., Hut, P. & Inagaki, S. 1987, ARAA, 125, 565
Fall, S. & Rees, M. 1985, ApJ, 298, 18
Goldstein, H. 1980, Classical Mechanics, (Reading, Mass: Addison-Wesley), p.383
Harris, W. E. 1991, ARAA, 29, 543
Harris, W. E. & Pudritz, R. E. 1994, ApJ, 429, 177
Heggie, D. C., & Ramamani, N., 1995, MNRAS, 272, 317
Henon, M., 1961, Ann. d'Astrophys., 24, 369
Hernquist, L. & Ostriker, J. P. 1992, ApJ, 386, 375
Hesser, J. E., 1993, in The Globular-Cluster Galaxy Connection, eds. Smith, G. H. & Brodie, J. P., (Astr. Soc. Pacific: San Francisco)
Inagaki, S., in Dynamics of Star Clusters, eds. Goodman, J., and Hut, P., (Boston: D. Reidel Publishing)
Inagaki, S & Saslaw, W. 1985, ApJ, 292, 339
King, I. R., 1962, AJ, 67, 471
Krall, N. A., & Trivelpiece, A. W. 1973, Principles of Plasma Physics, (New York: McGraw-Hill)
Landau, L. D., & Lifschitz, E. M. 1965, Quantum mechanics, non-relativistic theory, (London: Pergamon Press)
Larson, R. B. 1990, PASP, 102, 709
Larson, R. B. 1994, preprint
Lee, H. M. & Goodman, J. 1995, ApJ, 443, 109
Lee, H. M. & Ostriker, J. P. 1987, ApJ, 322, 123
Lee, H. M., Fahlman, G. G., & Richer, H. B. 1991, ApJ, 366, 455
Lichtenberg, A., & Lieberman, M. 1983, Regular and Stochastic Motion, (New York: Springer-Verlag)
Lightman, A. & Shapiro, S. 1978, Revs. Mod. Phys., 50, 437
Lynden-Bell, D. & Kalnajs, A. 1972, MNRAS, 157, 1
Lynden-Bell, D. & Wood, R. 1968, MNRAS, 138, 495
Murray, S. D. & Lin, D. N. C. 1992, ApJ, 400, 265
Oh, K. S. & Lin, D. N. C. 1992, ApJ, 386, 519
Okazaki, T. & Tosa, M. 1995, MNRAS, 274, 48
Ostriker, J. P.1985, in Dynamics of Star Clusters, eds. Goodman, J., and Hut, P., (Boston: D. Reidel Publishing)
Ostriker, J. P., Spitzer, L., Jr. & Chevalier, R. 1972, ApJL, 176, L51
Richer, H. B., & Fahlman, G. G. 1989, ApJ, 339, 178
Rosenbluth, M. N., MacDonald, W. M. & Judd, D. L. 1957, Phys-Rev, 107, 1
Spitzer, L., Jr. 1987, Dynamical Evolution of Globular Clusters, (Princeton: Princeton Univ. Press)
Spitzer, L., Jr. & Hart, M. 1971, ApJ, 164, 399
Spitzer, L., Jr. & Chevalier, R. A. 1973, ApJ, 183, 565
Stix, T. H. 1992, Waves in Plasmas, (New York: AIP Press)
Szebehely, V. 1967, Theory of Orbits, (New York: Academic Press)
Titchmarsh, E. C. 1986, Introduction to the Theory of Fourier Integrals, (New York: Chelsea Publishing Company)
Tremaine, S. D. & Weinberg, M. W. 1984, MNRAS, 209, 729
Weinberg, M. D. 1994, AJ, 108, 1414
Zinn, R., 1993, in The Globular-Cluster Galaxy Connection, eds. Smith, G. H. & Brodie, J. P., (Astr. Soc. Pacific: San Francisco)

APPENDIX A: DERIVATION OF TIDAL POTENTIAL

In the inertial Galactocentric frame, the coordinate components of a cluster star are

$$\vec{R} = \vec{r} + \vec{R}_{com}, \tag{A1}$$

and its velocity components are

$$\vec{V} = \vec{v} + \vec{V}_{com}, \tag{A2}$$

where $\vec{r}$ and $\vec{v}$ are the coordinates and velocities of the member star measured relative to the cluster center of mass and $\vec{R}_{com}$ and $\vec{V}_{com}$ are the center-of-mass position and velocity of the cluster. The Hamiltonian for an individual star in these coordinates is therefore

$$H_0' = \frac{1}{2}|\vec{V}|^2 + \Phi_c(|\vec{R} - \vec{R}_{com}|) + \Phi_R(|\vec{R}|) \tag{A3}$$

We introduce coordinates centered on the cluster with axes fixed in space through a canonical transformation using a generating function of the second kind (Goldstein 1985). This function can be written

$$F_2(\vec{R}, \vec{v}, t) = (\vec{v} + \vec{V}_{com}) \cdot (\vec{R} - \vec{R}_{com}) + f(t) \tag{A4}$$

where $f(t)$ is an arbitrary function of time. The transformation obeys the conditions $V_i = \partial F_2/\partial R_i$ and $r_i = \partial F_2/v_i$, thus satisfying Hamilton's principle. The new Hamiltonian $H_0 = H_0' + \partial F_2/\partial t$ so that (assuming the summation convention throughout)

$$H_0 = \frac{1}{2}|\vec{v}|^2 + \Phi_c(|\vec{r}|) + \Phi_G(|\vec{r} + \vec{R}_{com}|) - \left.\frac{\partial \Phi_G}{\partial R_i}\right|_{R_{com}} r_i - \frac{1}{2}|\vec{V}_{com}|^2 + \frac{\partial f}{\partial t}. \tag{A5}$$

Expanding the Galactic tidal potential about the center of mass, we obtain

$$H_0 = \frac{1}{2}|\vec{v}|^2 + \Phi_c(|\vec{r}|) + \Big[\frac{1}{2}\left.\frac{\partial^2 \Phi_G}{\partial R_i R_j}\right|_{R_{com}} r_i r_j + ...\Big] + \Big[-\frac{1}{2}|\vec{V}_{com}|^2 + \Phi_G(|\vec{R}_{com}|)\Big] + \frac{\partial f}{\partial t}. \tag{A6}$$

The term in the second pair of brackets is an arbitrary function of time which arises as an ambiguity in canonical transformations (Goldstein 1985). We note that it equals $-L_{com}$, the negative Lagrangian of the center-of-mass motion and that it can be eliminated by an appropriate choice of f. In this case, setting $f = \int L dt$ (the action associated with the center-of-mass motion) gives the desired form of the Hamiltonian for a star in the cluster frame:

$$H_0 = \frac{1}{2}|\vec{v}|^2 + \Phi_c(|\vec{r}|) + \Big[\frac{1}{2}\frac{\partial^2 \Phi_G}{\partial R_i R_j}\Big|_{R_{com}} r_i r_j + ...\Big]. \quad \text{(A7)}$$

In the expansion of the tidal potential, we can ignore all but the lowest-order term because successive terms are proportional to $(|\vec{r}|/|\vec{R}_{com}|)^{n-2}$ $(n = 3, ...)$ relative to the second order term and, therefore, fall off quickly due to the small size of a cluster compared to the size scale of the Galaxy. We are thus left with the quadratic approximation to the Galactic tidal field. The expression for the perturbing potential, equation (8), is obtained by evaluating this term of the expansion for the specific case of the logarithmic sphere.

APPENDIX B: PERICENTRIC INNER LAGRANGE POINTS

To obtain an expression for the pericentric inner Lagrange point, it is convenient to first transform to rotating coordinates having one axis aligned with the galactocentric radius of the cluster on its orbit. We omit the details of the transformation here and simply give the expression for the effective potential at pericenter in the rotating frame:

$$\Phi_{eff} = \Phi_c(|\vec{r}|) + \frac{1}{2}\Omega_0^2(R_p)\big[|\vec{r}|^2 - 2x^2\big] - \frac{1}{2}|\vec{\Omega_p} \times \vec{r}|^2. \quad \text{(B1)}$$

The first term is the cluster potential. The second term is the quadratic tidal potential for the logarithmic sphere transformed to a rotating coordinate system. The last term is the centrifugal potential arising from the angular frequency of rotation at pericenter. The quantity Ω_p is the pericentric angular frequency of the cluster orbit while $\Omega_0(R_p)$ is the angular frequency of a circular orbit at the pericentric radius which defines the tidal strain.

The pericentric inner Lagrange point x_p occurs at the instantaneous inflection point in the effective potential which lies along the galactocentric radius of the cluster. We derive an expression for x_p by considering the balance of forces which is implied by the effective potential. Taking the gradient, and considering the instantaneous point of equilibrium along the Galactocentric radius gives

$$\frac{GM(x_p)}{x_p^2} = \Omega_p^2 x_p + \Omega_0^2(R_p) x_p, \quad \text{(B2)}$$

where the left-hand side gives the cluster force while the right-hand side gives the centrifugal force and tidal strain, respectively.

To derive an expression for the inner Lagrange point in terms of R_a/R_p, we first rewrite the angular frequencies Ω_p and $\Omega_0(R_p)$ in terms of the angular frequency of a circular orbit at apocenter $\Omega_0(R_a)$. Using conservation of angular momentum between apocenter and pericenter gives

$$\Omega_p = J/R_p^2 = \Omega_a \left(\frac{R_a}{R_p}\right)^2 = \eta \Omega_0(R_a)\left(\frac{R_a}{R_p}\right)^2, \quad \text{(B3)}$$

where η denotes the ratio of the angular frequency of the orbit to the angular frequency of a circular orbit with the same apocenter. The flat rotation curve defines

$$\Omega_0(R_p) = \frac{V_0}{R_p} = \Omega_0(R_a)\big(\frac{R_a}{R_p}\big), \quad \text{(B4)}$$

and substituting into equation (B2) and solving for x_p, we obtain

$$x_p^3 = \frac{GM(x_p)}{2\Omega_0^2(R_a)}\left\{\frac{1}{2}\left(\frac{R_a}{R_p}\right)^2\left[\eta^2\left(\frac{R_a}{R_p}\right)^2 + 1\right]\right\}^{-1}. \quad \text{(B5)}$$

Now we define the effective pericentric angular frequency

$$\Omega_p'^2 = \Omega_0^2(R_a)\left\{\frac{1}{2}\left(\frac{R_a}{R_p}\right)^2\left[\eta^2\left(\frac{R_a}{R_p}\right)^2 + 1\right]\right\} \quad \text{(B6)}$$

where $\kappa = \eta e^{(1-\eta^2)/2}$ for the logarithmic sphere.

APPENDIX C: DERIVATION OF FLUX EQUATION

The flux equation, equation (9), can be derived from the $\langle f_2 \rangle$ formalism given in Weinberg (1994). The function $\langle f_2 \rangle$ defines the externally induced change in the distribution function. The general form for $\langle f_2 \rangle$ is

$$\langle f_2 \rangle = \sum_{\mathbf{l}} \mathbf{l} \cdot \frac{\partial}{\partial \mathbf{I}} \mathrm{W}_{\mathbf{l}}(\mathbf{I}), \quad \text{(C1)}$$

where we have performed the phase-averaging to derive the perturbation as a function of the actions. The quantity $W_{\mathbf{l}}(\mathbf{I})$ is a scalar function of the actions

$$W_{\mathbf{l}}(\mathbf{I}) = \frac{1}{2}\big(\mathbf{l} \cdot \frac{\partial \mathrm{f}_0}{\partial \mathbf{I}}\big)|\mathrm{U}_{\mathbf{l}}|^2 |\mathrm{a}(\mathbf{l} \cdot \mathbf{\Omega})|^2, \quad \text{(C2)}$$

where $a(\mathbf{l} \cdot \mathbf{\Omega})$ is a Fourier coefficient given by

$$a(\mathbf{l} \cdot \mathbf{\Omega}) = \int_{\mathrm{t}_0}^{\mathrm{t}} \mathrm{dt}' \mathrm{e}^{\mathrm{i}\mathbf{l}\cdot\mathbf{\Omega}\mathrm{t}'} \mathrm{g}(\mathrm{t}') \quad \text{(C3)}$$

and other quantities are as defined in §2.

To derive the flux equation we note that $\langle f_2 \rangle$ can be written as a divergence:

$$\langle f_2 \rangle = \sum_{\mathbf{l}} \nabla \cdot \mathbf{W}_{\mathbf{l}} \quad \text{(C4)}$$

where $\mathbf{W}_{\mathbf{l}} = \mathrm{W}_{\mathbf{l}} \times \mathbf{l}$. This equation makes number conservation manifest in action space.

To implement this term in a 1-dimensional Fokker-Planck scheme, we must change variables from actions to $(E, \kappa, \cos\beta)$ and average over κ and $\cos\beta$ to obtain the one-dimensional flux in energy space. The transformation can be performed easily using the covariant form of the equation (e.g. Rosenbluth et al 1957).

The divergence written in covariant form is

$$V^{\mu}_{,\mu} = \frac{1}{\sqrt{g}}\frac{\partial}{\partial x^{\mu}}\sqrt{g} V^{\mu} \quad \text{(C5)}$$

where V^{μ} is a contravariant vector and g is the determinant of the metric tensor, equal to the square of the Jacobian. Using this equation, we transform to the new $(E, \kappa, \cos\beta)$ coordinates, which we denote using primes. Transforming the contravariant vector $\mathbf{W}_{\mathbf{l}}$ gives

$$\mathbf{W}_\mathbf{l}' = \mathrm{W_l}(\mathbf{l}\cdot\mathbf{\Omega})\widehat{\mathrm{E}} + \mathrm{W_l}\left(\frac{\mathrm{l_2}}{\mathrm{J_{max}(E)}} - \frac{\mathrm{l_1}\kappa}{\Omega_1\Omega_{2\mathrm{max}}}\right)\widehat{\kappa} + W_\mathbf{l}\frac{l_3}{\kappa J_{max}(E)}\widehat{\cos\beta}, \quad \text{(C6)}$$

where the quantity $W_\mathbf{l}$ is the function defined above but now written in terms of the new variables. $\mathbf{W}_\mathbf{l}'$ is the function equivalent to $\mathbf{W_l}$ in the new coordinates.

Noting that the Jacobian is

$$\sqrt{g} = \kappa J_{max}^2(E)/\Omega_1. \quad \text{(C7)}$$

we may write $\langle f_2\rangle$ in the new coordinates:

$$\langle f_2\rangle = \sum_\mathbf{l}\frac{\Omega_1}{\kappa J_{max}^2}\nabla\cdot'\left(\frac{\kappa J_{max}^2}{\Omega_1}\mathbf{W}_\mathbf{l}'\right). \quad \text{(C8)}$$

Averaging over $(\kappa, \cos\beta)$

$$\langle\langle f_2\rangle\rangle = \frac{\int d\kappa d\cos\beta\kappa J_{max}^2/\Omega_1\langle f_2\rangle}{\int d\kappa d\cos\beta\kappa J_{max}^2/\Omega_1}, \quad \text{(C9)}$$

gives the total change as a function of energy:

$$\langle\langle f_2\rangle\rangle = \frac{\int d\kappa d\cos\beta\kappa J_{max}^2/\Omega_1\partial\big(\sum W_\mathbf{l}(\mathbf{l}\cdot\mathbf{\Omega})\big)/\partial\mathrm{E}}{\int \mathrm{d}\kappa\mathrm{d}\cos\beta\kappa\mathrm{J}_{\mathrm{max}}^2/\Omega_1}, \quad \text{(C10)}$$

where the fluxes in the $\widehat{\kappa}$ and $\widehat{\cos\beta}$ directions vanish due to the averaging. Fully expressed, the equation reads

$$\langle\langle f_2\rangle\rangle = \left\{\frac{1}{2}\sum_\mathbf{l}\frac{\partial}{\partial E}\Big[\int d\kappa\Big(\mathbf{l}\cdot\frac{\partial \mathrm{f_0}}{\partial\mathbf{I}}\Big)(\mathbf{l}\cdot\mathbf{\Omega})|\mathrm{U_l}|^2|\mathrm{a}(\mathbf{l}\cdot\mathbf{\Omega})|^2 \kappa J_{max}^2/\Omega_1\Big]\right\}\left\{\int d\kappa\kappa J_{max}^2/\Omega_1\right\}^{-1} \quad \text{(C11)}$$

The phase space volume

$$16\pi^2 P(E) = (2\pi)^3\int\frac{\kappa J_{max}^2}{\Omega_1}d\kappa, \quad \text{(C12)}$$

which we substitute to find the total phase space flux

$$\langle\langle f_2\rangle\rangle = (16\pi^2 P(E))^{-1}\frac{\partial}{\partial E}\{\langle\langle E\rangle\rangle\}. \quad \text{(C13)}$$

In the asymptotic limit, this becomes the rate of change of the phase space density, equation (9).

APPENDIX D: IMPLEMENTATION

The rate of change in the distribution function due to external heating is given by equation (9). We write this in finite difference form for consistency with the Fokker-Planck scheme and solve after each diffusion step. The numerical implementation uses a flux-conserving finite-difference scheme with explicit time advance:

$$\frac{f_j^{n+1} - f_j^n}{\Delta t} = -\frac{1}{P_j}\left\{\frac{\mathcal{F}_{j+1/2} - \mathcal{F}_{j-1/2}}{\Delta E}\right\}, \quad \text{(D1)}$$

where the flux $\mathcal{F}$ is denoted

$$\mathcal{F}_{j+1/2} = R_{j+1/2}\frac{df}{dE}, \quad \text{(D2)}$$

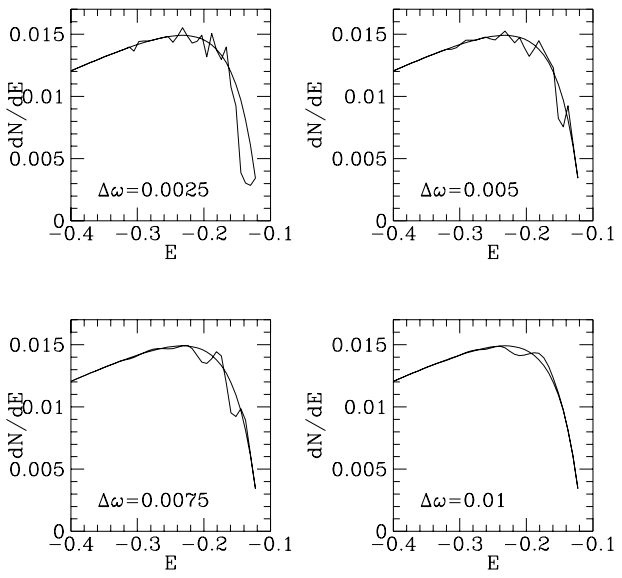

Figure D1. Increasing grid spacing corresponds to broadening resonances for the resonant heating calculation. Broader resonances spread the input power over a range of energies. As a result, the DF evolves more slowly and does not develop strong resonant peaks and troughs. Here we evolve the DF in a fixed potential

and we have rewritten the previously defined heating rate as

$$\langle\langle\dot{E}\rangle\rangle = R(E)\frac{df}{dE}. \quad \text{(D3)}$$

The function $R(E)$ represents the sum over all resonances which couple to orbits of energy E.

In equation (8), δ-functions denote resonant coupling of internal and external orbital frequencies. However, the resonant interaction has finite duration due to non-linear saturation or detuning which corresponds to a width in frequency space. For weak perturbations, narrow resonances develop since orbital frequencies evolve slowly. For strong perturbations large widths occur because frequencies evolve rapidly.

The grid spacing employed in the difference scheme defines the frequency widths. Wider spacing implies broader resonances. Broader resonances reduce the heating rate by smearing the input power over a wide region in phase space as shown in Figure D1. To estimate the proper grid spacing, we use the bandwidth theorem or uncertainty relation (e.g Bracewell 1986). The bandwidth theorem identifies the reciprocal relationship between the frequency width and sampling time of an oscillator:

$$\Delta\omega = \frac{2\pi}{\Delta t}. \quad \text{(D4)}$$

Here the sampling time is the duration of resonance. Since non-linearity develops with some typical change in energy δE, we use the rate of energy input to estimate the duration of resonance:

$$\Delta t = \frac{\delta E}{\dot{E}}. \quad \text{(D5)}$$

Comparisons with simulation indicate that 10% change in energy typically leads to frequency evolution. We calibrate the appropriate frequency widths using fully self-consistent N-body calculations described in Appendix E. For typical heating rates in tidally limited clusters, an initial spacing of $\Delta\omega = \Delta\mathbf{l}\cdot\mathbf{\Omega} \sim 0.005$ is appropriate. We use this value for all tidally-limited calculations. Larger tidal truncations require an increased width.

Two final implementation issues are the boundary conditions on the external heating equation and the Fokker-Planck equation. For the boundary conditions on equation (D1), we set the flux to zero at the center and the gradient of the flux to zero at the edge. The latter condition represents evaporation. The last grid point of the DF therefore stays fixed between each diffusion step. We tested the choice in outer boundary condition using a zero flux condition and found solutions which differed by a few percent at most.

We use the standard tidal boundary condition in the Fokker-Planck equation. This calls for truncating the distribution function at the maximum energy allowed by the tidal limit. Because strict application of the boundary condition calls for truncating the cluster at x_p, we would throw out a potentially large fraction of the initial cluster distribution in cases where $M(x_p) < 1$. As a less extreme alternative, we place the zero-DF boundary at the initial limiting energy of the cluster and set the heating rate according to our choice of x_p. Then we allow the boundary to evolve according to the mass loss. Tests with N-body calculations shown in Appendix E indicate that the prescription works correctly.

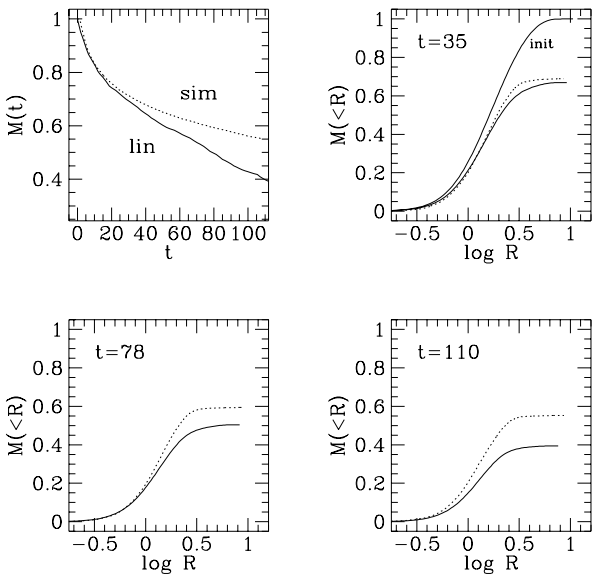

Figure E1. A $W_0 = 5$ cluster on a circular orbit with $M(x_p) = 0.95$. The half-mass dynamical time $t_{dyn} = 0.3$ and the orbital period is 2π. The top left panel shows the total mass as a function of time while the remaining panels show the mass profile at the indicated times. Agreement is good for $100t_{dyn}$. Deviation at later times results from inherent non-linearity and relaxation.

APPENDIX E: COMPARISON WITH SIMULATION

Comparisons of the external heating theory with N-body simulations are used to test linearity, the assumption of isotropy over long times, the importance of non-spherical moments in the potential, and the boundary condition on the heating equation (equation D1) and to calibrate frequency widths of heating rates. We use a self-consistent field expansion code (e.g. Hernquist & Ostriker 1992) with 1.5×10^4 particles, radial expansion order $n = 10$ and angular order $l = 4$. Figures E1 and E2 show comparisons for $\kappa = 1.0$ and $\kappa = 0.3$ orbits. The two methods agree fairly well, especially at early times, before non-linearity and relaxation produce differences at later times.

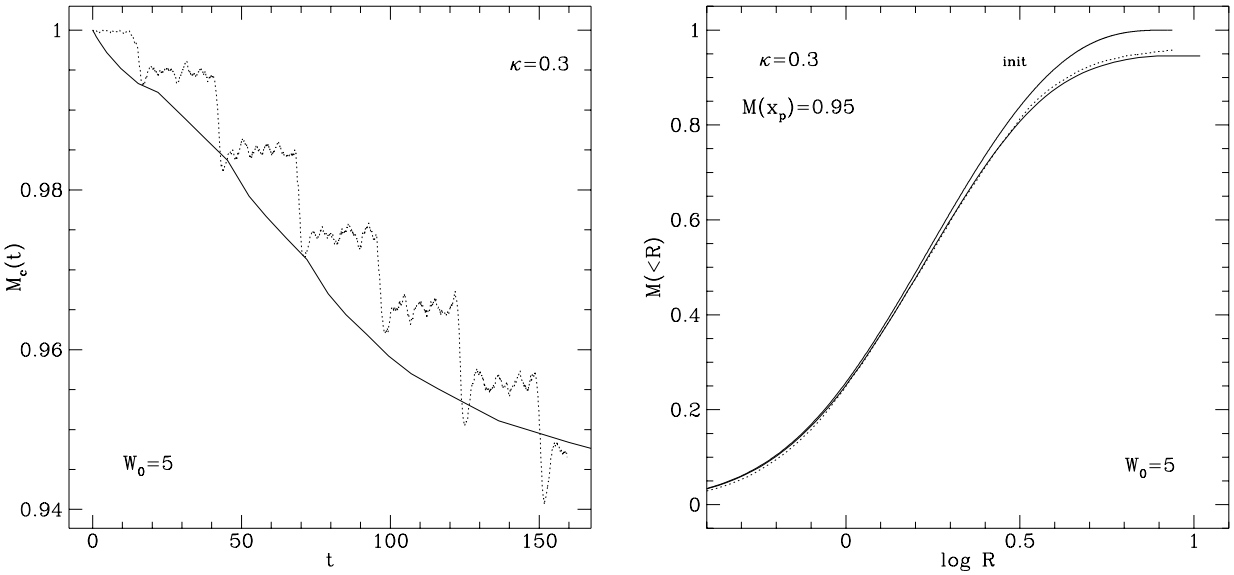

Figure E2. The same cluster as above on a $\kappa = 0.3$ orbit with $M(x_p) = 0.95$. The orbital period is $t = 30$. The left panel shows the evolution in total mass while the right panel compares the mass profiles at $t = 145$ or $483t_{dyn}$. Agreement is good over this duration.